JOURNAL OF CATALYSIS **159,** 410–417 (1996)
ARTICLE NO. 0104

In Situ Electrical Characterization of Magnesium Vanadate Reference Phases (meta-MgV_2O_6, pyro-$Mg_2V_2O_7$, and ortho-$Mg_3V_2O_8$) Used in Oxidative Dehydrogenation of Propane to Propene

V. Soenen,*,† J. M. Herrmann,*,[1] and J. C. Volta†

*URA au CNRS Photocatalyse, Catalyse et Environnement, Ecole Centrale de Lyon, B.P. 163, 69131, Ecully Cedex, France; and
†Institut de Recherches sur la Catalyse, CNRS, 2 Avenue A. Einstein, 69626, Villeurbanne Cedex, France

Received September 1, 1995; revised November 21, 1995; accepted November 30, 1995

The three meta-, pyro-, and orthomagnesium vanadate phases have been synthesized, characterized, and tested as catalysts in the oxydehydrogenation of propane. *In situ* electrical conductivity measurements have clearly indicated that these solids behave as intrinsic semiconductors in oxygen at reaction temperature (520°C), with band gap energies equal to twice the corresponding activation energies of conduction, in good agreement with the values determined by UV–visible spectroscopy. In the presence of propane, the electrical conductivity of the samples increased instantaneously at a variation rate and to an extent which both changed in the following order: pyro-$Mg_2V_2O_7$ > meta-MgV_2O_6 > ortho-$Mg_3V_2O_8$. The increase of conductivity has been attributed to the consumption of surface lattice oxygen anions by propane, leading to the formation of propene, water, and ionized anionic vacancies. The existence of these vacancies was supported by the study of their filling, using either dioxygen O_2 or nitric oxide NO, as sources of dissociated oxygen species. It is proposed that pure magnesium vanadates act as redox relays in the oxydehydrogenation of propane according to a Mars and van Krevelen mechanism. The higher catalytic activity of pyrovanadate $Mg_2V_2O_7$ is directly connected with the lability of its surface O^{2-} ions detected by conductivity. The high reoxidation rate implies that the solids are working in a surface state close to stoichiometry, i.e., close to the oxidized state. This could explain why the reaction kinetic order with respect to oxygen was equal to zero. The electrical properties of the three V–Mg–O phases could explain why pyrovanadate $Mg_2V_2O_7$ was the most active and the most selective phase for oxidative dehydrogenation of propane into propene.

INTRODUCTION

The selective conversion of alkanes to unsaturated hydrocarbons or to useful intermediates is a potentially important way to increase the chemical value of paraffins. Oxidative dehydrogenation in which water is formed as a by-product is not limited by thermodynamic equilibrium in the way that dehydrogenation is and it also avoids cracking of hydrocarbons, which reduces the selectivity of the reaction. As a consequence, the oxidative dehydrogenation of light alkanes using oxygen as the oxidizing agent appears to be more promising for industry than direct dehydrogenation. However, the oxidative dehydrogenation of alkanes usually produces a considerable amount of carbon oxides because of the low selectivity of the catalysts employed. The key aspect of the technology is, therefore, the development of catalysts capable of activating only the C–H bonds of the alkane molecule in a flow of oxygen, in order to improve selectivity. This problem is important due to the tendency of the petrochemical industry to use alkanes as raw materials directly instead of alkenes (1).

In this strategy, vanadium-containing oxides have been extensively studied. Indeed, it has been observed that the catalytic behavior of the supported vanadia depends on the nature of the support, changing the proportion of both isolated and associated vanadate species (2).

The oxidative dehydrogenation of light alkanes (particularly propane (3–6) and butane (6, 7)) has been investigated by different research groups on V–Mg–O oxide catalysts. In this case, mixed V–Mg–O phases can be generated by changing the V/Mg ratio, the conditions of precipitation from their corresponding salts, and the temperature of calcination. Meta-MgV_2O_6, pyro-$Mg_2V_2O_7$, and ortho-$Mg_3V_2O_8$ vanadates have been identified simultaneously with the MgO phase. The nature of the active phase responsible for the formation of propene from propane differs with the authors. Chaar and co-workers (3, 7) attributed the active phase to magnesium orthovanadate ($Mg_3V_2O_8$), while Siew Hew Sam *et al.* (4) suggested that magnesium pyrovanadate (α-$Mg_2V_2O_7$) was the active phase. The highest selectivity for magnesium pyrovanadate has been related by these authors to its ability to stabilize V^{4+} ions associated with oxygen vacancies (8). This conclusion was supported by the easier reducibility of this phase (8, 9). The contamination by residual potassium was considered as a possible explanation for the contradiction mentioned between the two groups (10). As at least two

[1] To whom correspondence should be addressed.

0021-9517/96 $18.00

phases have been identified simultaneously in the working catalysts, it was also suggested that the selectivity of the magnesium orthovanadate should be improved by a coexisting pyrovanadate phase or an excess of magnesium oxide in intimate contact, considering some possible type of cooperation between separate phases (5). Another interesting result was reported by Corma *et al.* who observed a parallelism between the selectivity and the shift of the binding energy of surface oxygen as evidenced by XPS studies of the vanadium magnesium oxides (11): the higher the binding energy of the O 1*s* line, the higher its selectivity in propene. This means that the lower nucleophilicity of the oxygen species, the better the catalytic properties of V–Mg oxides for the oxidative dehydrogenation of propane.

Active sites for oxidative dehydrogenation of propane are generally considered to be tetrahedral vanadium species, but there are different opinions concerning the detailed structure of the VO_4 surroundings. Some researchers (11, 12) relate the selectivity in propene to the presence of isolated VO_4 tetrahedra as in magnesium orthovanadate, while others (4) are in favor of corner-sharing VO_4 tetrahedra. According to this second approach, it has been proposed that the bridging oxygen atoms in the V–O–V bond for the magnesium pyrovanadate could be removed during the reaction generating two V^{4+} cations. This should give rise to a dynamic model in which the local structure should change from the V_2O_7 unit to two edge-sharing square-based VO_3 units (12). This model should explain the high dehydrogenation selectivity of the magnesium pyrovanadate by the stabilization of the V^{4+} ions associated with oxygen vacancies.

Although a number of investigations have been carried out on the V–Mg–O system, it is clear that an improvement in the catalytic behavior requires a further development of the fundamental knowledge of the different pure phases, especially a much deeper investigation of the reaction dynamics and its correlation with the nature of the surface, particularly in *in situ* conditions.

In the present work, the three pure magnesium vanadate phases (meta-$Mg_2V_2O_6$, pyro-$Mg_2V_2O_7$, and ortho-$Mg_3V_2O_8$) have been synthesized and characterized by electrical conductivity measurements. The electrical conductivity technique has been selected in this case because of the following advantages:

(i) it is a nondestructive analytic tool which can be used in experimental conditions similar to those of the oxidative dehydrogenation of propane, using the same temperatures and the same partial pressures of reactants (13);

(ii) the samples can be studied as powders without special pretreatments, all the catalyst grains being accessible to gaseous reactants;

(iii) correlations can be established with other techniques, particularly with UV–visible spectroscopy.

EXPERIMENTAL

1. *Preparation of the Reference V–Mg–O Phases*

Reference phases were prepared from magnesium hydroxide and ammonium vanadate (NH_4VO_3, Merck) according to a procedure which has been previously described (4).

$Mg(OH)_2$ was prepared by precipitation from a magnesium chloride solution ($MgCl_2 \cdot 6\ H_2O$, Merck, 0.25 *M*) (100 ml) by potassium hydroxide (Prolabo, 0.5 *M* (100 ml). After a first washing with distilled water, the precipitate was centrifuged and then dried under vacuum at 80°C. The solid thus obtained was freed from any residual chloride ions by washing repeatedly with water until the filtrate had a constant electrical conductivity. The solid was then dried under vacuum at 100°C and immediately used for the preparation of the V–Mg–O precursors of the pure V–Mg–O phases in order to avoid any further carbonation. An appropriate amount of $Mg(OH)_2$ powder was then added to a basic aqueous solution (1% NH_4OH) containing NH_4VO_3. For example, for the preparation of $Mg_3V_2O_8$, 114 ml of the NH_4VO_3 solution (0.5 *M*) were added to 5 g of fresh $Mg(OH)_2$. The suspension was evaporated to dryness while being stirred and then finally dried at 100°C. This solid was designated as 60 VMgO (chem. anal.: 58.5 V_2O_5 wt%). Magnesium vanadate reference phases were prepared from V–Mg–O precursors with different V/Mg ratios and designated henceforth as *x*VMgO (*x* corresponding to different V_2O_5 weight contents). For more details, see Ref. (4).

Trace amounts of potassium were detected by chemical analysis on the resulting solids but the K content was always less than 0.02%.

Magnesium orthovanadate $Mg_3V_2O_8$ was prepared from the 60 VMgO precursor (chem. anal.: 58.5 V_2O_5 wt%) calcined in air for 6 h at 550°C, 49 h at 625°C, 60 h at 640°C, 15 h at 750°C, and finally for 15 h at 800°C. It was ground between each heating. The XRD spectrum was characteristic of the $Mg_3V_2O_8$ phase in good agreement with the ASTM file (14). The purity has been estimated to be 95% with a slight impurity of β-$Mg_2V_2O_7$ (15, 16).

α-Magnesium pyrovanadate $Mg_2V_2O_7$ was prepared from a 69 VMgO precursor (chem. anal.: 66.4 V_2O_5 wt%) calcined in air for 6 h at 550°C, 6 h at 600°C, 6 h at 650°C, and finally for 17 h at 700°C. It was ground between each heating. The XRD spectrum was in good agreement with that observed by Clark and Morley (16). The purity has been estimated to be 95% with a slight impurity amount of β-MgV_2O_6.

β-Magnesium metavanadate MgV_2O_6 was prepared from a 82 VMgO precursor (chem. anal.: 79.8 V_2O_5 wt%) calcined in air for 6 h at 500°C, 6 h at 600°C, and 24 h at 700°C. It was ground between each heating. The XRD spectrum was in good agreement with the ASTM files (17–18).

TABLE 1

Characteristics of the V–Mg–O Reference Phases

V–Mg–O reference phases	Surface area (m^2/g)	Composition (wt%)			
		V (wt%)		Mg (wt%)	
		Theor.	Exp.	Theor.	Exp.
$Mg_3V_2O_8$	0.9	34.0	34.1	24.0	22.5
α-$Mg_2V_2O_7$	1.7	38.9	39.3	18.3	17.1
β-MgV_2O_6	0.1	46.0	45.9	11.0	10.3

The purity has been estimated to be 98% with a slight impurity of the low-temperature form of α-MgV_2O_6 (16).

The wt% composition and the surface areas of the reference V–Mg–O phases are listed in Table 1. There is a good agreement between the experimental and the theoretical composition.

2. *Characterization of the Reference Phases*

The reference phases were identified by X-ray diffraction. Experiments were performed using Cu$K\alpha$ radiation on a Siemens goniometer equipped with a quartz front monochromator. Textural measurements were performed on an automatic apparatus homemade at the Institut de Recherches sur la Catalyse (area and porosity determination). UV–visible spectra (diffuse reflectance) were recorded on a Perkin–Elmer Lambda 9 spectrometer equipped with an integration sphere.

3. *Electrical Conductivity Measurements*

The semiconductivity of the three magnesium vanadates has been investigated by using a cell specially designed to study electronic interactions between powdered samples and various atmospheres (13). Measurements were performed on sieved materials (250–420 μm). Around 0.4 g of catalyst was introduced between two platinum electrodes, where it was compressed under a constant pressure of ca. 10^5 Pa. The temperature of each electrode was given by a thermocouple whose wires were also used as conductors for electrical measurements. The electrical resistance of the samples was measured with various Ω-meters according to the range measured: a Kontron multimeter (model DMM 4021) for resistances lower than 2×10^6 Ω or with a digital teraohmmeter (Guildline Instruments, model 9520) for higher values. It was shown previously that powdered semiconducting oxides behave as massive conductors and the electrical conductivity of the powdered samples can be formally written as

$$\sigma = (1/R) \times (t/S),$$

where R is the electrical resistance and t/S is the geometric factor. Here t is the thickness (generally comprised between 0.3 and 0.5 cm) and S is the section area of the electrodes (diameter = 1.00 cm). Conductivity measurements carried out on powders do not provide intrinsic bulk values for the material, unlike experiments carried out on single crystals. However, they can give a good estimate of the variations of the concentration of the main charge carriers as a function of physical parameters such as temperature, oxygen pressure, nature, and pressure of reducing gases.

The procedure was the following. The samples were first outgassed at room temperature for 10 min and then put in contact with 400 Torr oxygen. The temperature was increased to 520°C corresponding to the temperature used in catalysis at a heating rate of 5°C/min. The initial reference state was that obtained under these conditions when the electrical conductivity remained constant. The electrical conductivity was then studied as a function of temperature and oxygen pressure. When sequences were performed under different atmospheres of pure gases, the gas phase of the preceeding sequence was promptly outgassed at the same temperature and replaced by the new gas phase previously prepared in the gas line. The electrical conductivity was permanently measured during all the operations. Propane and oxygen were purchased from Air Liquide with 99.95 and 99.9995% purity, respectively.

4. *Catalytic Measurements for Propane Oxidative Dehydrogenation*

The catalytic test was performed in a flow system which has already been described (4). The reference V–Mg–O phases were deposited on a fixed bed in a quartz microreactor (U-tube, 13 mm diameter) operating under atmospheric pressure. The catalytic zone was isothermal (6 mm height, 0.8 cm^3 volume) with a precatalytic (1.7 cm^3) and a postcatalytic (0.4 cm^3) zone. Analysis of reactants and reaction products was made by on-line gas chromatography. For the permanent gases and H_2O, a Delsi IGC 120 MB gas chromatograph equipped with a thermal conductivity detector was used. Hydrogen was the carrier gas. Two columns were operated in parallel, a 3 m 1/4 in. molecular sieve 5A column to separate O_2 and CO and a 2 m 1/4 in. Porapak column to separate CO_2 and H_2O. For the organic products, a Delsi IGC 120 FB gas chromatograph equipped with a flame ionization detector was used. Nitrogen was the carrier gas. Three columns were operated in parallel: (i) a 4 m 1/8 in. Durapak column to separate light hydrocarbons (methane, ethane, ethene, propane, propene), (ii) a 3 m 1/8 in. Carbowax column to separate oxygenates (ethanal, propanal, acetone, acrylaldehyde), and (iii) a 2 m 1/8 in. AT 1200 column to separate acids (acetic, propionic, and acrylic acids). This last column was situated in a furnace together with the four different injection valves which were monitored by a Spectra Physics computer. The reactor was directly connected to the furnace to prevent any condensation of the reaction products.

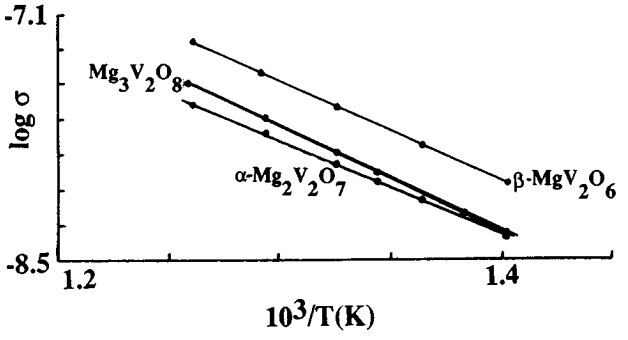

FIG. 1. Plot of log $\sigma = f(1/T)$ for the electrical conductivity of the three vanadate phases. Curve 1, MgV_2O_6; curve 2, $Mg_2V_2O_7$; curve 3, $Mg_3V_2O_8$. $P_{O_2} = 400$ Torr; σ in $\Omega^{-1} \cdot cm^{-1}$.

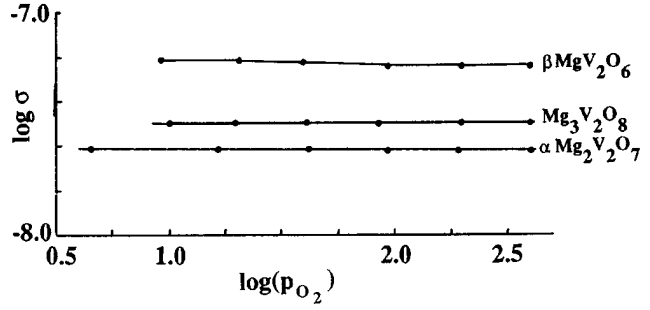

FIG. 2. Log–log plot of σ variations as a function of oxygen pressure at 520°C. Curve 1, MgV_2O_6; curve 2, $Mg_2V_2O_7$; curve 3, $Mg_3V_2O_8$. (P_{O_2} in Torr; σ in $\Omega^{-1} \cdot cm^{-1}$).

Under standard conditions, the feed was 2 vol% propane (99.99%, Air Liquide), 19.6% O_2, and 78.4% N_2. The flow rate was 3 liter/h. The empty reactor showed no activity (0.63% propane conversion at 550°C).

RESULTS AND DISCUSSION

The electrical conductivity σ of the three V–Mg–O reference phases has been measured as a function of various parameters (temperature, partial pressure of oxygen, and atmosphere of propane and of oxygen under pressures close to those used in catalysis) in order to provide evidence on the electron transfers, creation of defects, and redox processes which are involved in the catalytic oxidative dehydrogenation of propane.

1. Influence of Temperature

Temperature was varied in the range 440–520°C, where the solids are catalytically active. The variations of σ are presented in the form of a log σ vs $1/T$ plot given in Fig. 1. All the curves are straight lines whose slopes provide activation energies of conduction which are listed in Table 2. This means that the three solids behave as semiconductors in the temperature range investigated according to the law

$$\sigma = \sigma_0 \exp(-E_C/RT) \qquad [1]$$

TABLE 2

Activation Energies of Conduction and Band Gap Energies of the V–Mg–O Reference Phases

V–Mg–O reference phases	Activation energy of conduction (in kJ mol^{-1})	$\frac{d \log \sigma}{d \log P_{O_2}}$	E_G (from σ) (eV)	E_G (from UV–Vis) (eV)
$Mg_3V_2O_8$	114.5	0	2.38	2.34
α-$Mg_2V_2O_7$	105.8	0	2.20	2.21
β-MgV_2O_6	108.7	0	2.26	2.25

2. Influence of Oxygen Pressure

Oxygen pressure has been varied between 10 and 400 Torr at the temperature of 520°C. The variations of the electrical conductivity σ have been presented in the log–log plot of Fig. 2, in order to determine the exponent of P_{O_2}. This exponent can be equal to simple values which indicate the type of defects in equilibrium with gaseous oxygen or the nature of ionosorbed species (13). In the present case, the slopes of the diagram log $\sigma = f(\log P_{O_2})$ are equal to zero in the whole range of pressure investigated. This means that the partial order of oxygen in the following equation is nil:

$$\sigma = k \exp(-E_C/RT) P_{O_2}^0.$$

This also means that under the conditions used, there are no electron sources which are in equilibrium with gaseous dioxygen.

3. Consequences for the Semiconductor Nature of the V–Mg–O Phases

This behavior of the three V–Mg–O phases can be assumed to be similar to that of intrinsic semiconductors whose conduction electrons arise from the valence band, having been promoted into the conduction band provided their energy is larger than or equal to the band gap energy E_G. (Scheme 1).

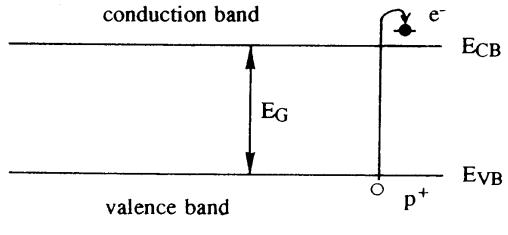

SCHEME 1. Energy band diagram of the VMgO intrinsic semiconductors.

The promotion of electrons from E_{VB} to E_{CB} can be represented by the equation

$$N \overset{K_2}{\leftrightarrows} e^- + p^+, \quad [2]$$

where N represents a neutral center and p^+ a positive hole in the valence band. The mass action law applied to Eq. [2] gives

$$K_2 = [e^-][p^+]. \quad [3]$$

The electroneutrality condition requires

$$[e^-] = [p^+]. \quad [4]$$

From Eqs. [3] and [4], there results

$$[e^-] = K_2^{1/2}, \quad [5]$$

where K_2 is the equilibrium constant of Eq. [2] and which follows van't Hoff's law

$$K_2 = (K_2)_0 \exp(-E_G/RT). \quad [6]$$

$(K_2)_0$ corresponds to the preexponential factor of the equilibrium constant K_2.

From Eqs. [5] and [6] one obtains

$$\sigma \propto [e^-] = (K_2)_0^{1/2} \exp(-E_G/2RT), \quad [7]$$

and by comparing Eqs. [1] and [7]

$$E_G = 2E_C. \quad [8]$$

The values of E_G, determined from E_C for the three V–Mg–O solids are reported in Table 2. These values have also been checked by UV–visible spectroscopy. It is known that photons whose energy $h\nu$ is larger than or equal to E_G can ionize an electron from the valence band into the conduction band at room temperature. This phenomenon is responsible for the photoconductivity of semiconductors (13, 19, 20). The UV–visible spectra of the three V–Mg–O reference phases have been recorded and an absorption threshold around 500–550 nm is indicated from Fig. 3. The absorption threshold is similar to the step function for single crystals. Presently, the three thresholds observed are very steep since the solids are not finely divided. The smaller the surface area (e.g., 0.1 $m^2\,g^{-1}$ for MgV_2O_6) (see Table 1), the steeper the absorption threshold. The band gap energies deduced from the spectra of Fig. 3 are listed in Table 2. They were deduced by the intersection of the linear decreasing part of the spectrum with the base line. They are in good agreement with the values determined from conductivity variations as a function of temperature. This is a good example of a convergent determination of a same physical parameter for a family of solids by two different physical techniques, one of electrical and the other of spectroscopic origin.

In conclusion, the three magnesium vanadates behave as intrinsic semiconductors, i.e., without surface defects generating electrons in equilibrium with gaseous oxygen. These solids are close to stoichiometry under pure oxygen at the reaction temperature used (520°C). Moreover, no ionosorbed oxygen species such as O_2^-(ads) , O^-(ads), or O^{2-}(ads) could be detected. O_2^-(ads) would have given σ variations as $P_{O_2}^{-1}$, O^-(ads) would have exhibited σ variations as $P_{O_2}^{-1/2}$, whereas O^{2-}(ads) species would have yielded σ variations as $P_{O_2}^{-1/4}$ (13) according to the respective equations:

$$O_2\ (g) + e^- \leftrightarrows O_2^-(ads)$$

$$1/2\ O_2\ (g) + e^- \leftrightarrows O^-(ads)$$

$$1/2\ O_2\ (g) + 2e^- \leftrightarrows O^{2-}(ads).$$

Since these solids are active in propane oxidative dehydrogenation, the surface reactivity has to involve surface O^{2-} anions from the lattice. This was checked by the experiments described in the next paragraph.

4. Electrical Conductivity under Propane and under Oxygen Atmospheres

The reactivity of lattice anions of the V–Mg–O reference catalysts has been evidenced by studying σ variations as a function of time in a propane atmosphere at a partial pressure equal to that used in catalysis (ca. 15 Torr). The variations are given in Fig. 4. Pyrovanadate $Mg_2V_2O_7$ exhibits the largest variations of more than 5 orders of magnitude, followed by metavanadate (MgV_2O_6), whereas the orthovanadate ($Mg_3V_2O_8$) conductivity varies only slightly. The final levels of conductivity reached after 2 h exposure to propane are indicative of the degree of reduction of the solids (8):

$$\text{pyro-}Mg_2V_2O_7 > \text{meta-}MgV_2O_6 > \text{ortho-}Mg_3V_2O_8.$$

Pyro-$Mg_2V_2O_7$ appears as the most reducible solid, in agreement with the study of the reduction by hydrogen (Fig. 1 in Ref. (8)). There is an inversion between the two other phases. This could be due to several factors as the difference in the reducing agents (hydrogen vs propane) or the difference in apparatus (a dynamic flow system working at programmed temperature vs a static-type cell working at a constant temperature identical to that of the reaction). The slope $d \log \sigma/dt$ in Fig. 4 correlates with the rate of reduction. The same order of reactivity is observed.

After 2 h in propane, where only pyrovanadate has reached a stable final reduction state, if the solids are promptly outgassed and submitted to an oxygen pressure of 137 Torr O_2, the electrical conductivity instantaneously decreases and returns to its initial values determined during the previous initial sequence in oxygen. This reversibility

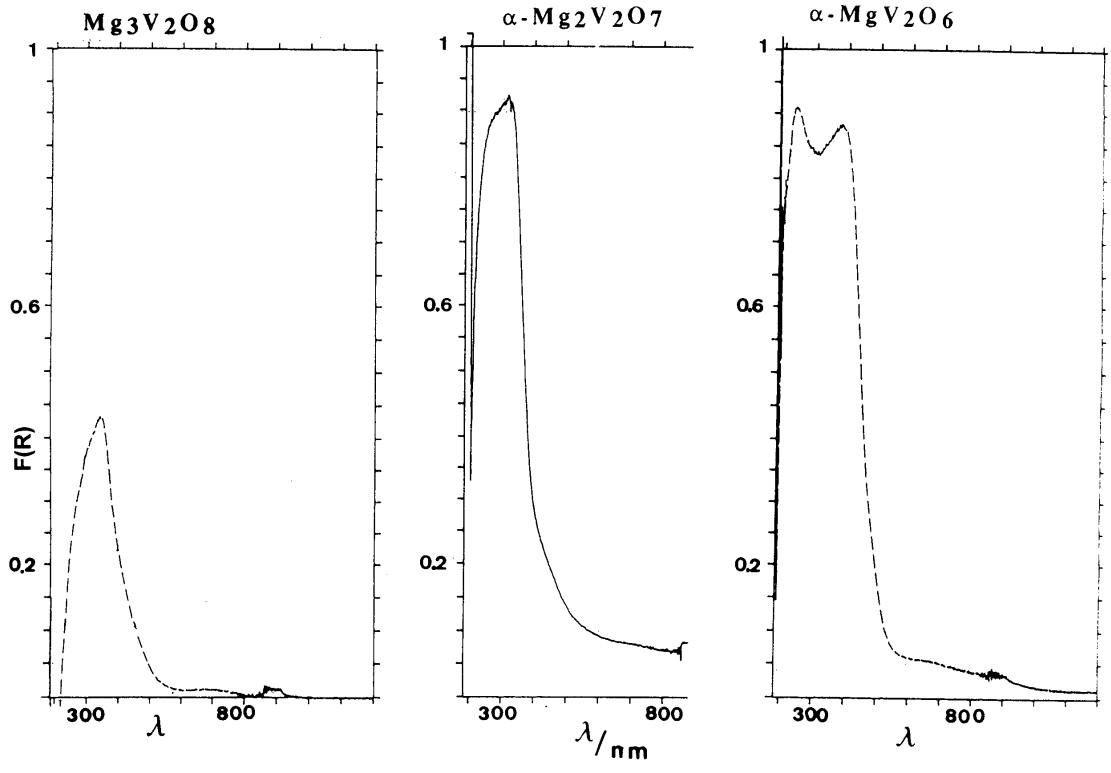

FIG. 3. UV–Visible reflectance spectra of the three V–Mg–O phases (Kubelka–Munk function $F(R) = f(\lambda)$).

confirms that the surface of the solids behaves as a reversible redox system. The slopes $(-d\sigma/dt)_{O_2}$, which are proportional to the reoxidation rates, vary in the order

$$\text{pyro-}Mg_2V_2O_7 > \text{meta-}MgV_2O_6 > \text{ortho-}Mg_3V_2O_8.$$

During the first sequence under propane, the increase of the electrical conductivity σ can be ascribed to the oxidative dehydrogenation reaction,

$$(O^{2-})^\circ + C_3H_8 \rightarrow C_3H_6 + H_2O + (V_{O^{2-}})^+ + e^-, \quad [9]$$

where $(O^{2-})^\circ$ is a lattice anion of V–Mg–O, which despite its two electrons is a neutral entity with respect to the solid and is indicated with a zero charge and where $(V_{O^{2-}})^+$ represents a singly ionized anionic vacancy. This vacancy is once positively charged with respect to the solid since it has lost one of the two electrons of the original anion $(O^{2-})^\circ$ disappeared.

In contrast, in the presence of oxygen O_2, this anionic vacancy can be filled with the capture of one electron:

$$(V_{O^{2-}})^+ + e^- + 1/2\,O_2(g) \rightleftarrows (O^{2-})^\circ \quad [10]$$

This explains the decrease of σ observed in Fig. 4.

The existence of anionic vacancies created by reduction of propane has been confirmed by adding another oxygen-containing molecule, NO, in contact with the reduced surface (Fig. 5). Instantaneously, a sharp decrease of σ is observed according to the equation

$$(V_{O^{2-}})^\circ + e^- + NO \rightarrow O^{2-} + N^\circ \xrightarrow[+NO]{+N^\circ} \begin{matrix} N_2 \\ N_2O \end{matrix} \quad [11]$$

These variations of conductivity enable one to find evidence for the existence of anionic vacancies in the reduced state, whereas these vacancies do not exist anymore under O_2. Since the absolute values of the slopes $d\sigma/dt$ observed in Fig. 4 are larger under oxygen than under propane, this means that the rates of reoxidation of the solids are higher

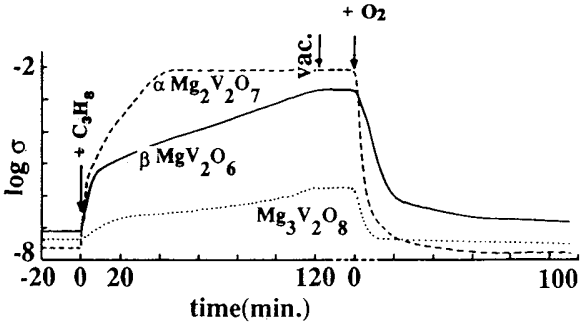

FIG. 4. Electrical conductivity variations at 520°C under reduction by propane (15 Torr) and subsequent reoxidation by O_2 (137 Torr).

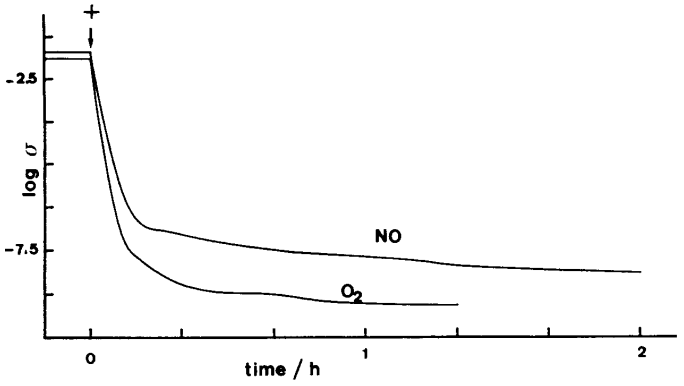

FIG. 5. Kinetics of the electrical conductivity σ (in $\Omega^{-1} \cdot cm^{-1}$) at 520°C during the filling of anionic vacancies by O_2 (137 Torr) and by NO (90 Torr) after a reducing pretreatment in propane (15.5 Torr for 15 min). The cross indicates the time when O_2 or NO were introduced after a prompt outgassing of propane.

than the rates of reduction. As a consequence, these solids have a surface close to the oxidized state during oxidative dehydrogenation of propane. In other words, the three V–Mg–O phases operate during reaction with a surface state close to stoichiometry.

5. *Consequence for Catalysis in Oxidative Dehydrogenation of Propane*

5.1. Redox process. As explained above, the three V–Mg–O reference phases do not exhibit surface defects such as anionic vacancies under pure oxygen. The anionic vacancies are only created by the reduction of the surface by propane (Eq. [9]) and their existence was evidenced by σ variations during the filling either by gaseous oxygen or by nitric oxide (Eqs. [10] and [11]). Additionally, electrical conductivity gave no evidence of oxygen ionosorbed species. Consequently, the only possibility which remains for a potential active species is the anion O_S^{2-} of the surface lattice of the solids. The anions are removed by propane according to Eq. [9], thus forming water, propene, and anionic vacancies. The surface anions O_S^{2-} are regenerated by the filling of the anionic vacancies according to Eq. [10]. This is a redox phenomenon occurring at reaction temperature (520°C). Since no adsorbed ionic oxygen species could be detected by conductivity, a Mars and van Krevelen mechanism (21) seems more probable than a Langmuir–Hinshelwood one. The catalyst appears as a redox relay able to lose some surface anions O^{2-} acting as oxidizing species. However, since these solids are intrinsic semiconductors with additionally low specific areas (Table 1), they have a very low tendency to lose their surface oxygen.

5.2. Comparison with catalytic performance. The catalytic performances of the reference V–Mg–O phases have been previously reported (4). Selectivities in C_3H_6, CO, CO_2, and oxygenated products were compared at similar conversion (7–8%). They are reported in Table 3.

TABLE 3

Catalytic Results for Propane Oxidative Dehydrogenation at 550°C on the V–Mg–O Reference Phases

V–Mg–O reference phases	Mass (g)	Conversion C_3H_8 (%)	Selectivity (%)			
			C_3H_6	CO_2	CO	Oxygenates
$Mg_3V_2O_8$	1.0	8.3	6.0	94.0	—	—
α-$Mg_2V_2O_7$	0.2	6.9	53.5	18.8	10.4	Acrylald. 12.0 Propanal 3.5 Acet. acid 1.0
β-MgV_2O_6	0.7	7.4	14.9	17.6	36.6	Ethanal 30.2

Note. Catalytic conditions: $C_3H_8/O_2/N_2$: 2/19.6/78.4, 760 Torr, 3 liter h^{-1}.

It appears that pyrovanadate $Mg_2V_2O_7$ is by far the most selective V–Mg–O phase for propene formation under the conditions indicated in Table 3. For this reason, it has been chosen to determine the kinetic law for propane oxidative dehydrogenation.

The rate r_1 of disappearance of propane is given by

$$r_1 = k_1 P_p^n \times P_{O_2}^0,$$

whereas that of propene formation r_2 is equal to

$$r_2 = k_2 P_p^m \times P_{O_2}^0.$$

The kinetic orders relative to oxygen are equal to zero. This is in agreement with what has been found for propane and butane oxidative dehydrogenation (3). This means that oxygen pressure has no influence upon the reaction rate. In the case of a hypothetical Langmuir–Hinshelwood mechanism, this would have meant that oxygen is working in adsorption conditions close to surface saturation. However, it was mentioned above that no ionic oxygen adsorbed. In the case of the Mars and van Krevelen mechanism, the zero kinetic order with respect to O_2 is indicative of a high oxidation rate of the solid, faster than the reduction one. This is in full agreement with the oxidation and reduction rates deduced from the initial slopes $d\sigma/dt$ of the σ curves in oxygen and in propane (Fig. 4).

Moreover, when one compares the curves of Fig. 4 with the catalytic results of Table 3, it can be deduced that the most reducible V–Mg–O phase, i.e., pyrovanadate, $Mg_2V_2O_7$, is the most selective in oxidative propane dehydrogenation. In contrast, orthovanadate $Mg_3V_2O_8$, which exhibits a small increase of conductivity under propane atmosphere, i.e., a low ability to lose lattice oxygen anions, is poorly selective in propene and mainly produces cracking oxidation with a high selectivity to CO_2. Metavanadate MgV_2O_6 has intermediate behavior with a low cracking activity providing some ethanal (Table 3).

It seems that the higher selectivity in propene for $Mg_2V_2O_7$ can be directly connected with the lability of its surface lattice oxygen ions.

CONCLUSIONS

Three pure reference phases of the V–Mg–O system (meta-$Mg_2V_2O_6$, pyro-$Mg_2V_2O_7$, and ortho-$Mg_3V_2O_8$) have been selected and tested by electrical conductivity.

From intrinsic semiconductors in oxygen at reaction temperature (520°C), they become *n*-type semiconductors under propane at the same temperature. This clearly demonstrates that active oxygen species are surface lattice anions whose departure from the surface (when oxygenates are evolved) creates anionic vacancies subsequently filled by gaseous oxygen. The three solids behave as reversible relays in propane oxidative dehydrogenation.

The comparison of the electrical behavior of the three V–Mg–O phases clearly indicates that pyro-$Mg_2V_2O_7$ is the most reactive phase in *in situ* conditions with the most numerous labile surface anions. This corroborates the catalytic results obtained in a differential flow reactor which indicate that $Mg_2V_2O_7$ is the most active and selective catalyst for propane oxidative dehydrogenation to propene. In addition, the higher value of the rate of oxidation of this solid as compared with its rate of reduction indicates a surface state close to oxygen stoichiometry and allows prediction of a zero kinetic order which has been confirmed.

From this study, it can be concluded that *in situ* electrical conductivity measurements constitute a powerful technique in oxidation catalysis, able to determine the nature of the oxygen active species, the oxidation state of the surface of the oxide catalyst, and the predicted kinetic order of oxygen.

ACKNOWLEDGMENT

The authors are indebted to Dr. D. Siew Hew Sam for the preparation of the pure V–Mg–O reference phases and to Mrs. M. Roullet and Mr. J. Disdier for technical assistance.

REFERENCES

1. Roth, J. F., *Chem. Tech.* **21**, 357 (1991).
2. Mamedov, E. A., and Cortés Corberan, V., *Appl. Catal.* **127**, 1 (1995).
3. Chaar, M., Patel, D., and Kung, H. H., *J. Catal.* **109**, 463 (1988).
4. Siew Hew Sam, D., Soenen, V., and Volta, J. C., *J. Catal.* **123**, 417 (1990).
5. Gao, X., Ruiz, P., Xin, Q., Guo, X., and Delmon, B., *J. Catal.* **148**, 56 (1994).
6. Corma, A., Lopez Nieto, J. M., Paredes, N., Dejoz, A., and Vazquez, I., *Stud. Surf., Sci. Catal.* **82**, 113 (1994).
7. Chaar, M. A., Patel, D., Kung, M. C., and Kung, H. H., *J. Catal.* **105**, 483 (1987).
8. Guerrero Ruiz, A., Rodriguez-Ramos, I., Fierro, J. L. G., Soenen, V., Herrmann, J. M., and Volta, J. C., *Stud. Surf. Sci. Catal.* **72**, 203 (1992).
9. Gao, X., Ruiz, P., Xin, Q., Guo, X., and Delmon, B., *Catal. Lett.* **23**, 321 (1994).
10. Kung, M. C., and Kung, H. H., *J. Catal.* **134**, 668 (1992).
11. Corma, A., Lopez-Nieto, J. M., and Paredes, N., *J. Catal.* **144**, 425 (1993).
12. Bouloux, J. C., Milosevic, I., and Galy, J., *J. Solid State Chem.* **16**, 393 (1976).
13. Herrmann, J. M., *in* "Catalyst Characterization" (B. Imelik and J. C. Védrine, Eds.), Chap. 20, p. 559. Plenum Press, New York, 1994.
14. ASTM file No. 19-779.
15. Wollast, R., and Tazairt, A., *Silic. Ind.* **34**, 37 (1969).
16. Clark, G. M., and Morley, R., *J. Solid State Chem.* **16**, 429 (1976).
17. Galy, J., and Pouchard, M., *Bull. Soc. Chim. Fr.* 261 (1967); ASTM file No. 23-1233.
18. ASTM file No. 34-13.
19. Bube, R. H., "Photoconductivity of Solids." Wiley, New York, 1960.
20. Rose, A., "Photoconductivité. Modéles et problémes annexes," Monographie Dunod, Paris, 1966.
21. Mars, P., and van Krevelen, W., *Chem. Eng. Sci., Spec. Sup.* **9**, 41 (1954).